Original Research

Loss of smooth muscle α-actin effects on mechanosensing and cell–matrix adhesions

MP Massett[1,*], BC Bywaters[2,*], HC Gibbs[3,*], JP Trzeciakowski[4], S Padgham[4], J Chen[5], G Rivera[2], AT Yeh[3], DM Milewicz[5] and A Trache[3,4]

[1]Department of Health and Kinesiology, Texas A&M University, College Station, TX 77843, USA; [2]Department of Veterinary Pathobiology, Texas A&M University, College Station, TX 77843, USA; [3]Department of Biomedical Engineering, Texas A&M University, College Station, TX 77843, USA; [4]Department of Medical Physiology, Texas A&M University Health Science Center, Bryan, TX 77807, USA; [5]Department of Internal Medicine, McGovern Medical School, University of Texas Health Science Center, Houston, TX 77030, USA
Corresponding author: A Trache. Email: trache@tamu.edu
*These authors contributed equally to the work.

Impact statement

Thoracic aneurysm formation is characterized by progressive enlargement of the ascending aorta, which predisposes the aorta to acute aortic dissection that can lead to sudden death. SMCs in the aorta play an integral role in regulating vessel wall contractility and matrix deposition in the medial layer. Recent studies show that mutations in genes associated with actomyosin apparatus reduce SMC contractility, increasing susceptibility to TAAD. Single-cell experiments enable discrete measurements of transient microscopic events that may be masked by a macroscopic average tissue behavior. Biophysical methods combined with microscopy techniques aid in understanding the specific roles of adhesion and cytoskeletal proteins in regulating SMC mechanosensing when SMα-actin is disrupted. Our findings suggest that *Acta2*$^{-/-}$ cells have increased SMγ-actin and decreased integrin recruitment at cell–matrix adhesion, hence a synthetic phenotype with reduced cellular mechanosensing.

Abstract

Mutations in *ACTA2*, encoding smooth muscle α-actin, are a frequent cause of heritable thoracic aortic aneurysm and dissections. These mutations are associated with impaired vascular smooth muscle cell function, which leads to decreased ability of the cell to sense matrix-mediated mechanical stimuli. This study investigates how loss of smooth muscle α-actin affects cytoskeletal tension development and cell adhesion using smooth muscle cells explanted from aorta of mice lacking smooth muscle α-actin. We tested the hypothesis that reduced vascular smooth muscle contractility due to a loss of smooth muscle α-actin decreases cellular mechanosensing by dysregulating cell adhesion to the matrix. Assessment of functional mechanical properties of the aorta by stress relaxation measurements in thoracic aortic rings suggested two functional regimes for *Acta2*$^{-/-}$ mice. Lower stress relaxation was recorded in aortic rings from *Acta2*$^{-/-}$ mice at tensions below 10 mN compared with wild type, likely driven by cytoskeletal-dependent contractility. However, no differences were recorded between the two groups above the 10 mN threshold, since at higher tension the matrix-dependent contractility may be predominant. In addition, our results showed that at any given level of stretch, transmural pressure is lower in aortic rings from *Acta2*$^{-/-}$ mice than wild type mice. In addition, a three-dimensional collagen matrix contractility assay showed that collagen pellets containing *Acta2*$^{-/-}$ smooth muscle cells contracted less than the pellets containing the wild type cells. Moreover, second harmonic generation non-linear microscopy revealed that *Acta2*$^{-/-}$ cells locally remodeled the collagen matrix fibers to a lesser extent than wild type cells. Quantification of protein fluorescence measurements in cells also showed that in absence of smooth muscle α-actin, there is a compensatory increase in smooth muscle γ-actin. Moreover, specific integrin recruitment at cell–matrix adhesions was reduced in *Acta2*$^{-/-}$ cells. Thus, our findings suggest that *Acta2*$^{-/-}$ cells are unable to generate external forces to remodel the matrix due to reduced contractility and interaction with the matrix.

Keywords: Integrins, actin, vascular smooth muscle cells, *Acta2*$^{-/-}$ mice

***Experimental Biology and Medicine* 2020; 245: 374–384. DOI: 10.1177/1535370220903012**

Introduction

Structural and functional integrity of the vessel wall is due, in part, to the crosstalk between the collagen and elastin rich extracellular matrix with vascular smooth muscle cells (SMCs). The matrix bears the majority of the mechanical stress in the aorta. SMCs sense this stress via cell–matrix adhesions. Thus, changes in transmural pulse pressure are sensed by integrin receptors on the cell surface at the interface with the matrix. Then, the mechanical stimulation is transmitted intracellularly to the actomyosin contractile unit inducing cellular adaptation to external stress (i.e. mechanosensing).

Dynamic rearrangement of actin cytoskeleton is necessary to redistribute physical forces needed for cell contraction that enables cell adaptation to the extracellular microenvironment.[1,2] Thus, external mechanical stresses are balanced by intracellular counter-forces provided by the actomyosin apparatus, which forms stress fibers[3,4] through the interaction with dense plaques (i.e. focal adhesions). These adhesion structures form at the cell membrane interface connecting the cell to the matrix.[5,6] Cell–matrix adhesions transfer mechanical perturbation to and from the matrix via integrin receptors.[2,7–11] SMCs express a variety of integrins (e.g. $\alpha1\beta1$, $\alpha2\beta1$, $\alpha5\beta1$, $\alpha v\beta3$) that contribute to cellular crosstalk with the extracellular matrix in the vessel walls. For example, $\alpha1\beta1$ and $\alpha2\beta1$ integrins bind with high affinity to collagen, while $\alpha5\beta1$ and $\alpha v\beta3$ integrins have specific roles in regulating contractile function.[12–15] *In vivo*, $\alpha5\beta1$ binding to the RGD sequence of matrix proteins induces vascular contraction,[16,17] while $\alpha v\beta3$ binding to RGD causes arteriolar relaxation.[18] However, both integrins are needed for arterial vasoconstriction in response to increased pressure.[15] In addition, RGD peptide treatment or functional inhibition of integrins $\alpha5\beta1$ and $\alpha v\beta3$ inhibits angiotensin II-induced arterial contraction.[15,19] *In vitro*, integrin $\alpha v\beta3$ has a major role in regulating cell migration, while $\alpha5\beta1$ is involved in SMC contractile phenotype.[20,21] Moreover, $\alpha v\beta3$ integrin binds with high affinity to fibrillin-1, the major component of elastin-associated microfibrils, mediating actomyosin-elastin crosstalk in the aortic wall.[22,23]

Taken together, these results suggest that integrin-mediated interaction of SMCs with extracellular matrix impacts vascular smooth muscle contractility. Dysfunctional components of this tightly regulated mechanism could reduce the integrity of the aortic wall and lead to thoracic aortic diseases such as aortic aneurysms.

Mutations in genes that encode contractile proteins in SMCs[24–30] induce decreased contractility and increased SMC proliferation.[31] Mutations in *ACTA2*, the gene encoding smooth muscle α-actin (SMα-actin), are the most frequent cause of nonsyndromic, heritable TAAD.[28,32] These mutations are associated with impaired SMC function that leads to decreased ability of the cell to sense matrix-mediated mechanical stimuli. In the current study, we utilize mice lacking *Acta2* ($Acta2^{-/-}$), an animal model used to study TAAD.[33] SMCs isolated from these mice exhibit the same general phenotype as SMCs from humans with *ACTA2* missense mutations: reduced contractility, but increased cell migration and proliferation.[33] Aortic tissue from $Acta2^{-/-}$ mice also show ascending aortic enlargement and increased medial area.[34] This study tested the hypothesis that reduced vascular smooth muscle contractility due to a loss of SMα-actin alters cellular mechanosensing by dysregulating cell adhesion to the matrix. Thus, we employed a combination of physiological and biophysical approaches to dissect the functional and morphological changes induced by loss of SMα-actin in the arterial wall. Our results suggest that SMCs from $Acta2^{-/-}$ mice have reduced contractility and are unable to generate external forces to remodel the matrix. Further, we showed that loss of SMα-actin induced compensatory upregulation of SMγ-actin, and reduced integrin recruitment at cell–matrix adhesions.

Materials and methods

Animals

All procedures adhered to the established National Institutes of Health guidelines for the care and use of laboratory animals and were approved by the Institutional Animal Care and Use Committee at The University of Texas at Houston. Mice were originally generated by inserting a Pol2NeobpA cassette between the promoter and the coding region of the *Acta2* gene to disrupt transcription.[35] Mice were subsequently bred onto a C57BL/6 background for more than 10 generations.[33] Mice were allowed ad libitum access to food and water and maintained on a 12-h light:dark cycle (7 a.m.–7 p.m.) in a controlled temperature (21–22 °C). Experiments were conducted using cells and tissues from male homozygous $Acta2^{-/-}$ mice and wild type (WT) littermates as controls.

Aortic ring preparation and stress relaxation

At 13 weeks of age, mice were anesthetized by intraperitoneal injection of Avertin (350 mg/kg). Thoracic aortas were dissected, placed in ice-cold Hanks' Balanced Salt Solution, and shipped overnight. As previously shown,[36–37] overnight storage does not affect the passive mechanical properties. Upon receipt, aortas were placed under a stereoscope and cleaned of excessive perivascular tissue before cutting them into 2 mm ring segments of equal length. Each ring segment was suspended in an organ chamber of a 610 M Multi Chamber Myograph System (Danish Myo Technology, Denmark) filled with 8 mL of oxygenated (95% O_2, 5% CO_2) physiological saline solution (118.31 mM NaCl, 4.69 mM KCl, 1.2 mM $MgSO_4$, 1.18 mM KH_2PO_4, 24.04 mM $NaHCO_3$, 0.02 mM EDTA, 2.5 mM $CaCl_2$, and 5.5 mM glucose) and allowed to equilibrate at 37°C for at least 30 min.

To assess the mechanical properties of the vessel, stress relaxation was assessed in thoracic aortic rings from $Acta2^{-/-}$ and WT mice. Aortic rings were stretched in 4 mN increments from 0 mN until the calculated transmural pressure of 13.3 kPa (100 mmHg) was attained. Transmural pressure was calculated as $p = 2\pi^*T/L$, where L is the internal circumference corresponding to wall tension T.[38] Length and tension were recorded immediately

after each 4 mN increase in tension and again after 1 min.[39,40] Stress relaxation was calculated as the difference between the 4 mN increase in tension and the tension after 1 min, and was expressed as a percent decrease in tension. Passive tension curves were generated by plotting calculated transmural pressure (kPa) versus tension (mN). A repeated measures ANOVA followed by Bonferroni post-hoc analysis was used to assess strain differences for stress relaxation and passive tension curves. All values are presented as mean ± SD. Statistical significance was evaluated at $P < 0.05$.

Vascular smooth muscle cell isolation and cell culture

Vascular smooth muscle cells were explanted from the ascending aorta from male *Acta2*$^{-/-}$ and WT littermates as previously described.[41] Cells were cultured in a 100 mm cell culture dish in Smooth Muscle Basal Media (PromoCell, Heidelberg, Germany) supplemented with 20% fetal bovine serum, 20 mM HEPES (Sigma-Aldrich, St. Louis, MO, United States), 2 mM L-glutamine, 1 mM sodium pyruvate, 100 U/mL penicillin, 100 mg/mL streptomycin, and 0.25 mg/mL amphotericin B, and set in an incubator at 37°C with 5% CO_2. Cells were then plated on 35 mm glass bottom dishes (MatTek, Ashland, MA, United States) coated with matrix proteins. Each dish was coated with 20 μg/mL of fibronectin (FN) (Sigma, Saint Louis, MO, United States), collagen I (Coll I) (Sigma, Saint Louis, MO, United States) or collagen IV (Coll IV) (Millipore, Billerica, MA, United States), incubated at 4°C overnight, and then washed with Dulbecco's phosphate-buffered saline (DPBS) before plating the cells. Cells plated on uncoated substrates were used as controls. Five hours after plating, cells were serum starved overnight in the same cell culture media with 1% FBS and all other supplements except growth factors prior to immunofluorescence staining. Low passage cells were used for imaging experiments. All reagents were purchased from Invitrogen (Carlsbad, CA, United States), unless otherwise specified.

Three-dimensional collagen matrix remodeling

Collagen gel preparation

A collagen solution was prepared using rat tail collagen type I (Corning, Corning, NY, United States) by following manufacturer's protocol. Cells were trypsinized, centrifuged, and then resuspended in phenol-free media. Then, the collagen solution was mixed with cells in suspension to obtain a final concentration of 150,000 cells/mL and 3.5 mg/mL collagen. The cell-seeded collagen gel was further adjusted to pH 7.3–7.6. A volume of 250 μL cell-seeded collagen gel was added to each well of a 48-well plate and further incubated at room temperature for 45 min. After this time, 500 μl of SMC culture medium was added to each well and the plate was placed in an incubator at 37°C with 5% CO_2 for 24 h. The cell-seeded collagen gel was then fixed in 4% paraformaldehyde and 5% sucrose in DPBS for imaging.[42]

Non-linear optical microscopy and image processing

Cells cultured in three-dimensional collagen gels and fixed as described above were imaged with a custom-built non-linear optical microscope that utilizes ultrashort, broadband, near-infrared pulses to achieve efficient two-photon excited fluorescence (TPEF) and second harmonic generation (SHG).[43] Briefly, 10-femtosecond pulses centered at 800 nm with a bandwidth of 133 nm from a Kerr-lens mode locked Ti:Sapphire (Spectra-Physics, previously Femtolasers, Vienna, Austria) were chirped with dispersion compensating mirrors (Femtolasers, Vienna, Austria) prior to telescopic expansion (Thorlabs, Newton, NJ, United States) and focusing through a 20×, 1.0 NA water immersion objective (Carl Zeiss, Thornwood, NY, United States). Dispersion compensation is required to ensure the pulses arrive at the focal plane near the transform-limit (all wavelengths in phase). The low-magnification, high-NA objective allows imaging over a large field of view without sacrificing image resolution. Point-by-point volumetric scanning was achieved with x-y mirrors driven by galvanometers (Cambridge Technologies, Cambridge, MA, United States), and z-drive stage controller (MAC 5000, Ludl Electronic Products, Hawthorne, NY, United States), for SHG and TPEF signals from the collagen and cells, respectively. Signals were collected in an epi-detection geometry, separated from the excitation laser with a 630 nm short pass filter. The two emission channels were split with a 430 nm dichroic mirror and further filtered with a 405/20 nm (collagen SHG) and 450/60 nm (for cells) bandpass filters and focused onto photomultiplier tube detectors (Hamamatsu, Bridgewater, NJ, United States) for single photon counting. Voxel dimensions were 0.5 μm × 0.5 μm × 0.5 μm resulting in volumes with an x-y field of view of 128 × 128 μm and variable depth. Optical filters were purchased from Chroma Technology Corporation (Bellow Falls, VT, United States) unless otherwise specified.

Quantification of cell-seeded collagen gel fluorescence images

Images were visualized with FIJI[44,45] and Vaa3D software.[46] Two-dimensional xy images of raw photon counts from individual optical sections were used for analysis with a custom Matlab program (Mathworks, Natick, MA, United States). Collagen fiber orientation was quantified with a Fourier approach that directionally filters the spatial frequencies of the image to create a distribution of fiber angles from 0 to 180°.[47] This quantification resulted in the calculation of an alignment index (AI) for the collagen fibers that was defined as the ratio of the fiber distribution within 20° of the dominant fiber angle to the value found within the same range of a random distribution.[48] Theoretically, AI varies from 1.0 for a random fiber distribution to 4.55 for parallel fibers. However, the experimentally measured range does not typically span the entire theoretical range. The AI values measured here are similar to those reported previously in other culture systems by us and other groups.[48–50] The difference between the AI values for WT and *Acta2*$^{-/-}$ cell-seeded collagen gels was tested

for significance with an unpaired, two-tailed *t*-test. Statistical significance was evaluated at $P < 0.05$.

Cell contraction assay

Cells were trypsinized, centrifuged, and then resuspended in phenol-free media. Two million cells in suspension were mixed with a collagen solution prepared using manufacturer's protocol (CBA-201, Cell Bio Labs, San Diego, CA, United States). The collagen-cell gel was added to each well of a 24-well plate and incubated at 37°C with 5% CO_2 for 48 h. The polymerized collagen matrix containing cells remains attached to the culture dish during contraction phase. Mechanical tension develops during contraction, and cellular stress fibers assemble leading to mechanical loading. After that time, a sterile flexible spatula was used to release the collagen from the sides and bottom of the wells. Releasing the cell-seeded collagen gel results in mechanical unloading and further contraction as mechanical stress dissipates.[51] The free-floating cell-seeded collagen gel was imaged at 4, 27, and 48 h using a Moticam 1000 camera (British Columbia, Canada) in bright field. The plate was quickly returned to the incubator after each time point. The experiment was performed in triplicate. The diameter of the free-floating cell-seeded collagen gel was then measured for each time point using scoring tools in FIJI software. Statistical significance was evaluated at $P < 0.05$.

Assessment of vascular smooth muscle cell architecture

Immunofluorescence staining

Vascular SMCs plated in glass bottom dishes (MatTek, Ashland, MA, United States) were fixed after 24 h by immersion in 2% paraformaldehyde in DPBS followed by washing in a glycine buffer. Cells were incubated overnight at 4°C with primary antibodies for rabbit anti-integrin $\alpha 2$ (Abcam, San Francisco, CA, United States) or rabbit anti-integrin $\alpha 5$ (Milipore-Sigma, Burlington, MA, United States) diluted in a sodium citrate buffer containing BSA and Triton X.[52] After washing, cells were incubated with goat anti-rabbit Alexa 568 secondary antibody (Invitrogen, Carlsbad, CA, United States) for 1 h at room temperature. Then, cells were washed again and immediately imaged in DPBS. A similar procedure was followed for primary antibody hamster anti-integrin $\beta 3$ pre-conjugated with Alexa 488 (BioLegends, San Diego, CA, United States) that was incubated overnight. The smooth muscle γ-actin (SMγ-actin) antibody[53,54] was a gift of Dr. Christine Chaponnier (Department of Pathology and Immunology, University of Geneva, Switzerland). To evaluate SMγ-actin, cells were first fixed with 1% paraformaldehyde in DPBS followed by permeabilization with cold methanol.[42] As described above, cells were then labeled with anti-SMγ-actin (IgG1) primary antibody in DPBS followed by goat anti-mouse IgG1 Alexa 488 secondary antibody (Jackson Immuno Research, West Grove, PA, United States).

Vascular smooth muscle cell imaging

Total internal reflection fluorescence (TIRF) microscopy was used to image integrins and point-scanning confocal microscopy was used to image actin. TIRF microscopy is based on the total internal reflection phenomenon that occurs when light passes from a medium with a high refractive index (i.e. glass) into a medium with a low refractive index (i.e. water).[55] At the interface between the two media, the light will bend and if the incident angle is higher than a threshold value, determined by the refractive media at the interface, then the light will turn back into the high refractive medium and only a short-range electromagnetic disturbance, called evanescent field, will pass into the low refractive medium. Since the evanescent field intensity decreases exponentially with distance from the interface, the excitation of the fluorescent labeled protein will take place only in the immediate vicinity of the interface, hence exciting the fluorophores at the basal cell level. Thus, this imaging method provides high-contrast images of the basal cell area, with a useful maximum depth of penetration of ~100 nm. A PLAN APO 60× oil 1.45 NA TIRF objective lens and a CoolSnap HQ camera (Photometrics, AZ) were used for imaging cell–matrix adhesions with an exposure time of 100 ms on a microscope system as previously described.[56]

Confocal images were acquired on a laser-scanning confocal microscope Olympus Fluoview FV3000 as 3D stacks of 26 planes at a 0.39 μm step size. To form a 2D image, the laser beam scans the fluorescent cell in a raster pattern, that is, horizontally and vertically, and the fluorescence light

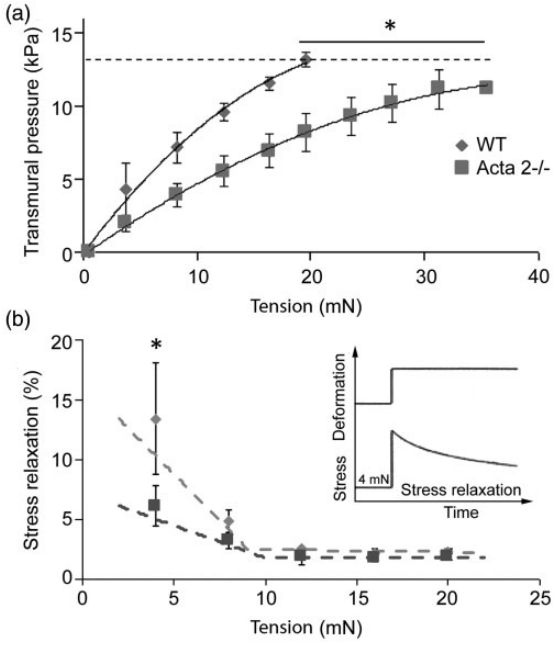

Figure 1. (a) Aortic rings stretched until a calculated transmural pressure of 13.3 kPa (100 mmHg) was attained (dashed line) showed that transmural pressure is lower in aorta from *Acta2*$^{-/-}$ mice compared with WT. (b) Thoracic aortic rings were sequentially stretched to elicit 4 mN increases in tension (see inset). Stress relaxation was significantly reduced at low tension in aorta from *Acta2*$^{-/-}$ mice compared with WT mice, while no significant difference was measured at tension values above 10 mN ($n = 4$ per group). Data shown as mean ± SD. *Significance was evaluated at $P < 0.05$.

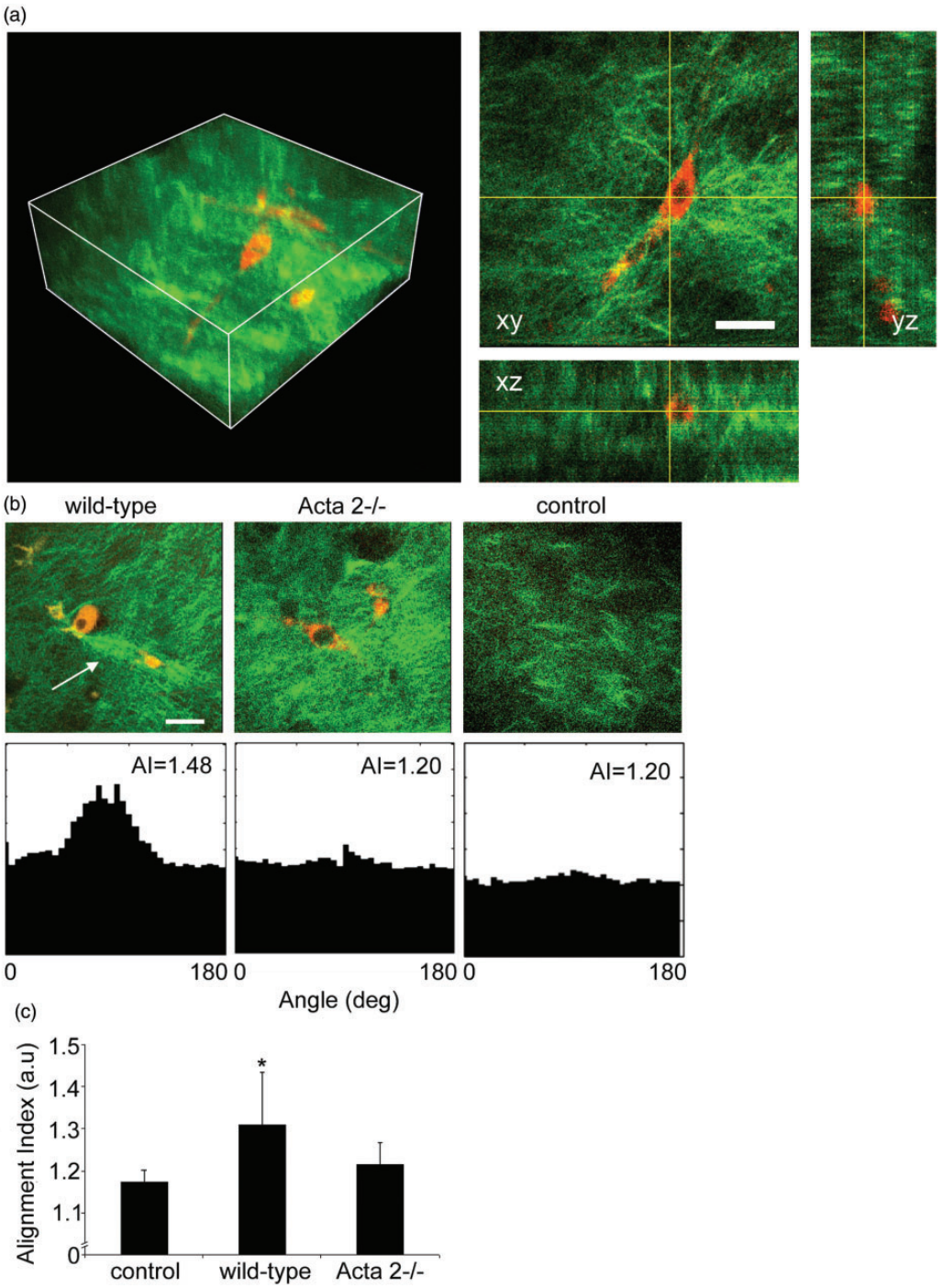

Figure 2. (a) Representative 3D image of cell-seeded collagen gel and 2D optical sections in xy, xz, and yz planes. Collagen was pseudo-colored in green (SHG signal), while SMCs were pseudo-colored in red (auto-fluorescence signal). (b) Representative 2D optical sections and their individual alignment angle distributions. Wild-type cells exert force on the collagen matrix inducing higher remodeling of the collagen fibers (see arrow), while *Acta2*$^{-/-}$ cells have reduced local matrix remodeling. (c) The distribution of collagen fiber orientation measured by the alignment index (AI) for WT cells shows a significant increase in respect to control (collagen gel without cells), while no change was recorded for *Acta2*$^{-/-}$ cells ($n = 10$–14 per condition). Scale bar represents 50 μm. Data shown as mean ± SD. *Significance was evaluated at $P < 0.05$.

emitted from the cell is detected by a low-noise photomultiplier tube detector and converted for 2D display on a computer screen. A PlanApo N SC2 60× oil, 1.4 NA objective lens was used for imaging actin filaments. Images were further analyzed as xy projections of the 3D stacks.

For both confocal and TIRF imaging of single cells, all hardware parameters were maintained the same throughout the experiments, respectively.

Fluorescence quantification

Fluorescence images were analyzed using the masking tool and image statistics tools in the SlideBook software (Intelligent Imaging Innovations, Denver, CO) as previously described.[20] Briefly, protein area for integrins at focal adhesions was determined from TIRF images, while 2D projections of confocal images were used to measure actin

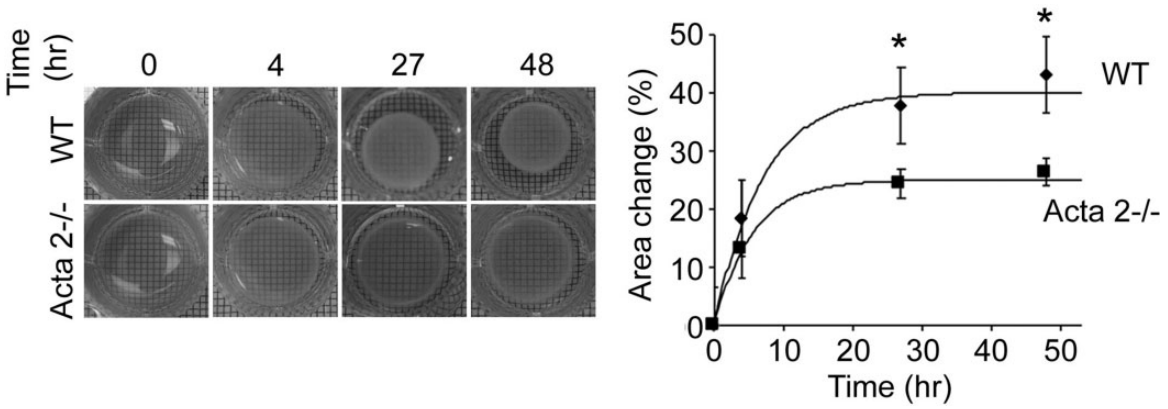

Figure 3. Free-floating cell-seeded collagen gel showed a reduced contractility for *Acta2*$^{-/-}$ vs. WT cells. Experiments were performed in triplicate. Data shown as mean ± SD. *Significance was evaluated at $P < 0.05$.

area throughout the cell. Fluorescence protein area measurements represent the relative protein density at the specific sites.[57] Since we compare a large number of cells for each condition, fluorescence protein area was normalized to total cell area for each cell before statistical analysis carried out with STATA (StataCorp, College Station, TX). Multiway analysis of variance (ANOVA) was used for statistical analysis. Planned comparisons between means were tested by orthogonal contrasts, and differences were considered significant at $P < 0.05$.

Results

Acta2$^{-/-}$ aorta has reduced stress relaxation

Figure 1(a) shows that at any given level of stretch, transmural pressure is lower in aorta from *Acta2*$^{-/-}$ mice. In addition, the internal circumference at a transmural pressure of 13.3 kPa was slightly larger for *Acta2*$^{-/-}$ (2906 ± 449 μm) than for WT (2428 ± 274 μm). Moreover, stress relaxation measured in *Acta2*$^{-/-}$ and WT mouse aortic rings shows two functional regimes for aortic tension (Figure 1(b)). Stress relaxation was significantly reduced at low tension in aorta from *Acta2*$^{-/-}$ mice compared with aorta from WT mice, while no significant difference was measured at tension values above 10 mN. These data suggest that vessel contractility is predominantly driven by SMCs at lower tension, and by matrix elasticity at higher tension. Taken together, these data support a reduced contractile phenotype associated with SMα-actin disruption and a dominant contribution of SMCs at lower tension.

Loss of SMα-actin decreases interaction of vascular smooth muscle cells with the matrix

Interaction between SMCs isolated from aortas of *Acta2*$^{-/-}$ or WT mice with the surrounding matrix was tested by embedding the cells in collagen I hydrogels. We performed non-linear optical microscopy on the cell-seeded collagen gels, capturing cellular two-photon excited autofluorescence and collagen SHG[48] to visualize the extent of cell-induced matrix remodeling in three-dimensions. Reconstructions of volumetric rendering are shown in Figure 2(a) with orthogonal optical sections from a representative image stack. Figure 2(b) shows that SMCs (red) from WT mice exert force on the collagen matrix (green) inducing extensive collagen fiber remodeling (see arrow), while no significant fiber remodeling was observed in collagen gels containing cells from *Acta2*$^{-/-}$ mice.

Quantitative assessment of collagen matrix remodeling (Figure 2(c)) showed that alignment index (AI) of fiber orientation increased for hydrogels containing WT cells, while no change was measured for hydrogels containing *Acta2*$^{-/-}$ cells with respect to control (no cells). In addition, a contractility assay[51] in which diameter of the free-floating cell-seeded collagen gel was measured shows a two-fold reduced contractility for *Acta2*$^{-/-}$ vs. WT cells ($P < 0.05$) (Figure 3). These results suggest that *Acta2*$^{-/-}$ cells are not able to generate the force needed to induce matrix remodeling necessary to maintain cellular contractility.

The architecture of the actin cytoskeleton and cell–matrix adhesions is differentially modulated in *Acta2*$^{-/-}$ aortic smooth muscle cells

While increased arterial stiffness is usually associated with aging and hypertension,[58,59] in patients predisposed to TAAD, aortic stiffness increases before aneurysm formation.[60] Contraction in vascular smooth muscle is driven by SMα-actin, the predominant actin isoform in SMCs, while SMγ-actin is less abundant in the vasculature.[61,62] Papke *et al.*[33] showed that pan-actin levels do not change in *Acta2*$^{-/-}$ SMCs compared to WT cells, in part due to increased expression of SMγ-actin mRNA. Thus, we sought to characterize cellular localization of SMγ-actin using fluorescence imaging. Confocal imaging of cells immunostained with a recently developed, specific SMγ-actin antibody[53,54] showed a significant increase of SMγ-actin throughout the cytoplasm in *Acta2*$^{-/-}$ compared with WT cells (Figure 4). *Acta2*$^{-/-}$ cells plated on fibronectin and collagen I showed similar levels of fluorescence for SMγ-actin, which were lower than for cells plated on collagen IV or control. Moreover, fine filaments of SMγ-actin are present in *Acta2*$^{-/-}$ cells plated on fibronectin and collagen I. These results suggest that loss of SMα-actin induces a compensatory increase in SMγ-actin that could

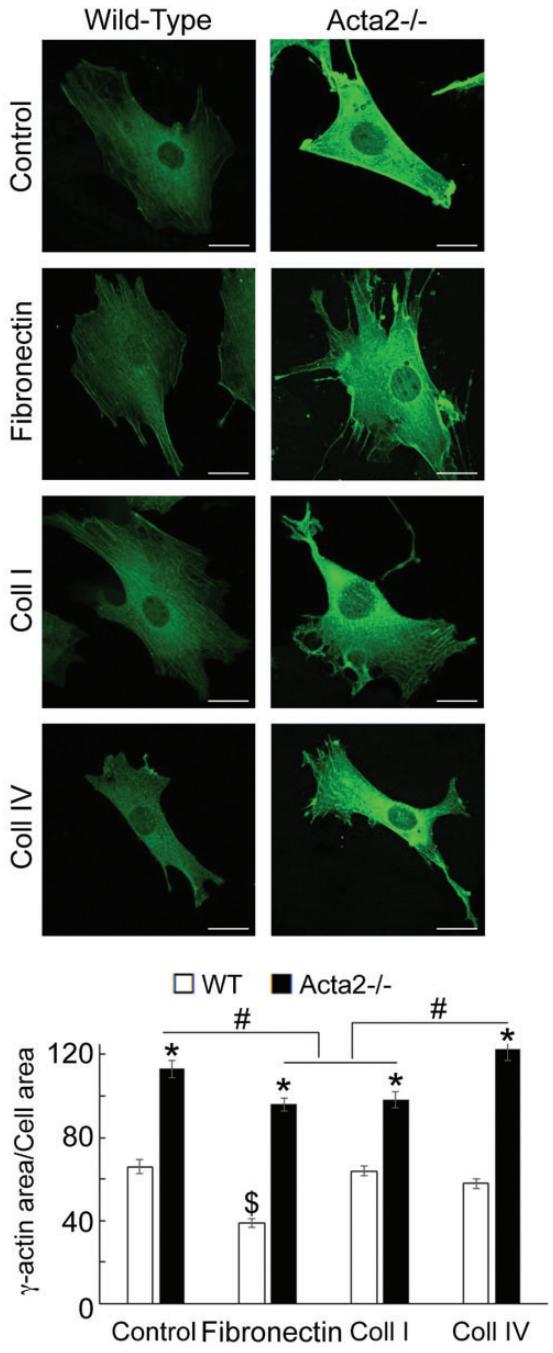

Figure 4. (a) Representative confocal images of SMγ-actin in *Acta2*$^{-/-}$ and WT cells plated on different extracellular matrices. Scale bar represents 20 μm. (b) Quantitative analysis of fluorescence images (n= 34–54 cells per condition). Data shown as mean ± SEM. Significance was evaluated at $P < 0.05$. *Significant difference between WT and *Acta2*$^{-/-}$ cells for each matrix, $ Significant difference between WT cells, # Significant difference between *Acta2*$^{-/-}$ cells as shown. (A color version of this figure is available in the online journal.)

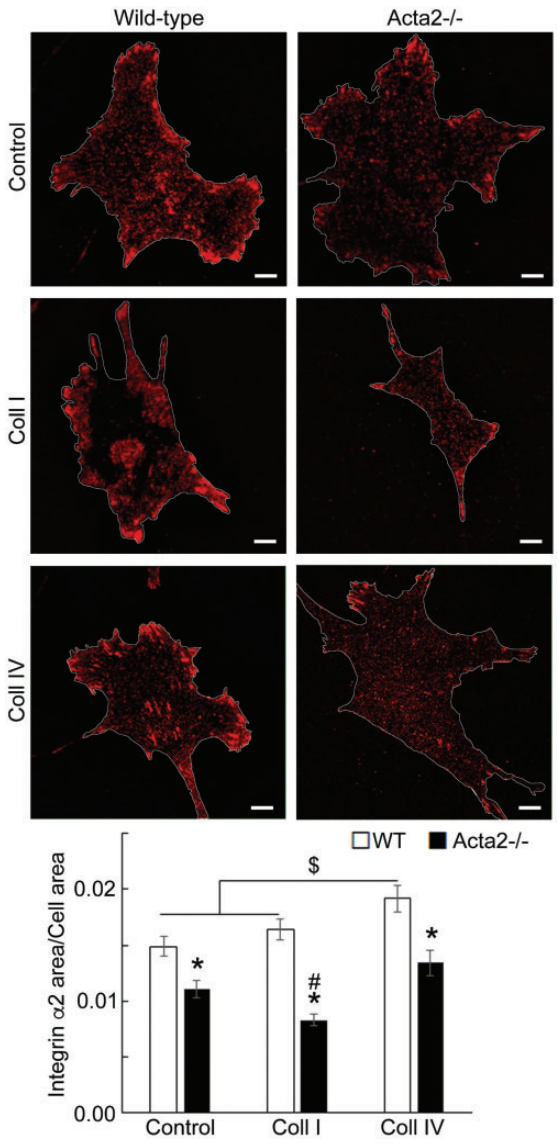

Figure 5. (a) Representative TIRF images of integrin α2 in *Acta2*$^{-/-}$ and WT cells plated on different extracellular matrices. Scale bar represents 10 μm. Cell periphery is outlined with a white line. (b) Quantitative analysis of fluorescence images (n = 29–49 cells per condition). Data shown as mean ± SEM. Significance was evaluated at $P < 0.05$. *Significant difference between WT and *Acta2*$^{-/-}$ cells for each matrix, $ Significant difference between WT cells as shown, # Significant difference between *Acta2*$^{-/-}$ cells. (A color version of this figure is available in the online journal.)

potentially contribute to increase stiffness of *Acta2*$^{-/-}$ cells,[33] but is not able to compensate and restore cellular contractile properties.

To further investigate whether SMα-actin disruption affects integrin-specific cell adhesion, immunofluorescence staining for integrin α2, α5 and β3, followed by TIRF microscopy was employed to characterize the morphology of cell–matrix adhesions. Fluorescence imaging showed that integrin α2 recruitment at cell–matrix adhesions takes place mostly at the cell periphery and was significantly lower in *Acta2*$^{-/-}$ cells compared with wild-type cells (Figure 5). Wild-type cells plated on collagen I or control showed similar levels of fluorescence for integrin α2, which were lower than for cells plated on collagen IV. Integrin α5 recruitment was significantly increased when both mutant and WT SMCs were plated on fibronectin (Figure 6). However, *Acta2*$^{-/-}$ cells presented lower integrin α5 localization at cell–matrix adhesions on uncoated, control substrates ($P < 0.05$), while WT cells presented strikes-like cell–matrix adhesions toward the center of the cell. *Acta2*$^{-/-}$ cells plated on fibronectin stimulated α5 integrin engagement in long streaks at the cell edges and towards the

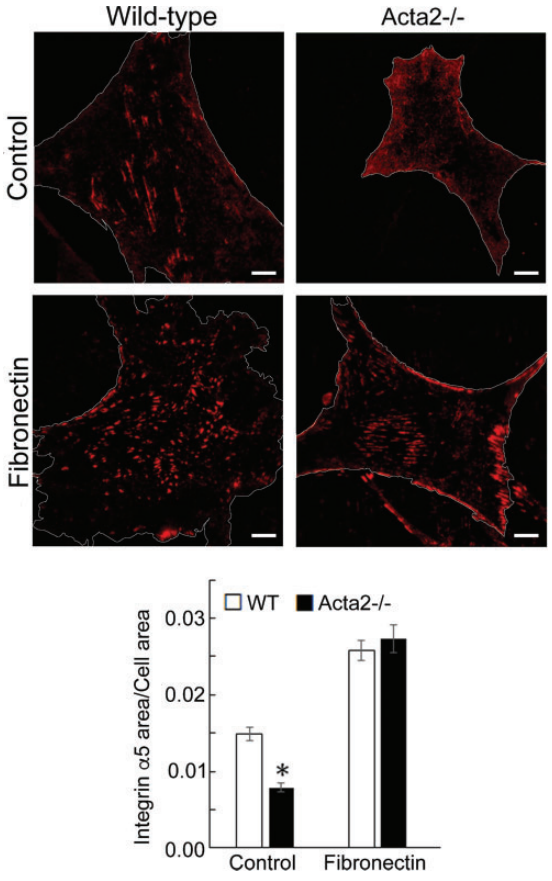

Figure 6. (a) Representative TIRF images of integrin $\alpha 5$ in *Acta2*$^{-/-}$ and WT cells plated on different extracellular matrices. Scale bar represents 10 μm. Cell periphery is outlined with a white line. (b) Quantitative analysis of fluorescence images ($n = 27$–35 cells per condition). Data shown as mean ± SEM. *Significance was evaluated at $P < 0.05$. (A color version of this figure is available in the online journal.)

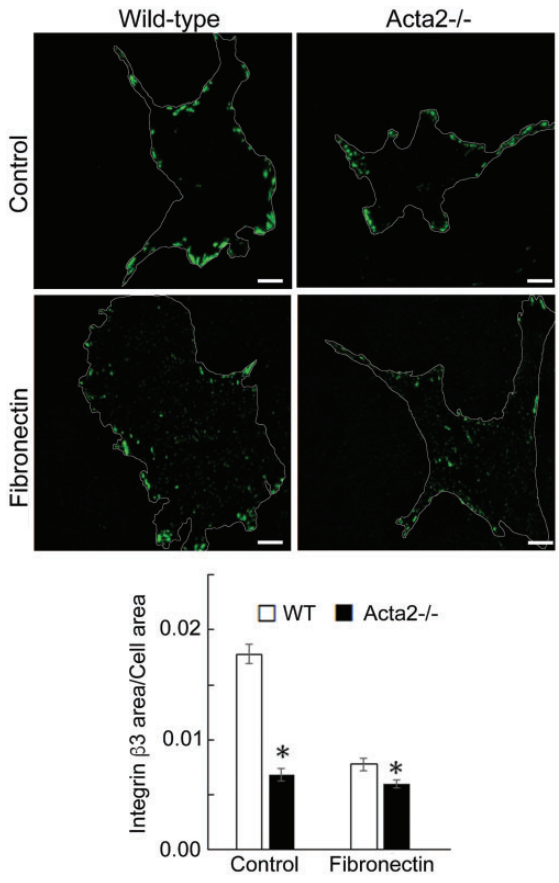

Figure 7. (a) Representative TIRF images of integrin $\beta 3$ in *Acta2*$^{-/-}$ and WT cells plated on different extracellular matrices. Scale bar represents 10 μm. Cell periphery is outlined with a white line. (b) Quantitative analysis of fluorescence images ($n = 28$–46 cells per condition). Data shown as mean ± SEM. *Significance was evaluated at $P < 0.05$. (A color version of this figure is available in the online journal.)

center of the cell. In contrast, WT cells plated on fibronectin induced robust recruitment of $\alpha 5$ integrin all over basal cell surface, mostly away from cell edges. Integrin $\beta 3$ recruitment at cell–matrix adhesions presented similar trend with integrin $\alpha 5$ on control, uncoated substrates; however, fibronectin has not increased $\beta 3$ integrin recruitment at cell–matrix adhesions (Figure 7). There was no significant difference between *Acta2*$^{-/-}$ cells plated on either substrate. As expected, integrin $\beta 3$ was localized exclusively at cell edges.[63] Cell–matrix adhesions were well defined for WT cells on uncoated, control substrates, and less organized for WT cells plated on fibronectin. *Acta2*$^{-/-}$ cells showed more diffuse adhesions when plated on either substrate.

These results show that loss of SMα-actin is associated with reduced integrin-binding to the matrix that concurs with increased cell migration and proliferation of *Acta2*$^{-/-}$ cells.[33]

Discussion

Smooth muscle cells in the aorta play an integral role in regulating vessel wall contractility and matrix deposition in the medial layer. Recent studies show that mutations in genes associated with actomyosin apparatus (i.e. *ACTA2*), reduce SMC contractility, increasing susceptibility to TAAD.[28–30] These mutations also are associated with impaired SMC function leading to decreased ability of the cell to sense matrix-mediated mechanical stimuli. This study investigates how loss of SMα-actin affects actin cytoskeleton and cell adhesions using an animal model of thoracic aortic aneurysm, the *Acta2*$^{-/-}$ mice.[35] Our results show that SMCs from *Acta2*$^{-/-}$ mice have reduced contractility and are unable to generate external forces to remodel the matrix. Further, we showed that loss of SMα-actin induced compensatory upregulation of SMγ-actin, and a reduction of integrin recruitment at cell–matrix adhesions.

Stress relaxation in smooth muscle represents a reduction in tension following a stretch and is thought to be involved in long-term regulation of blood pressure.[40] Our results from functional experiments performed in aortic rings showed that stress relaxation in *Acta2*$^{-/-}$ mice was reduced at lower tensions, presumably associated with cytoskeletal-dependent contractility. This is consistent with the finding that inhibition of actin polymerization with cytochalasin impairs stress relaxation in rat aorta.[40] Nagayama *et al.*[64] also demonstrated that the elastic component of stress relaxation was reduced by half in rat aortic smooth muscle cells treated with cytochalasin compared

with untreated SMCs. Collectively, these results suggest that remodeling of the actin-cytoskeleton contributes to stress relaxation.

The estimated transmural pressure at any level of stretch was significantly lower in aorta from *Acta2*$^{-/-}$ mice suggesting that the ability to generate circumferential tension in response to stretch is impaired in *Acta2*$^{-/-}$ mice. Our results also show increased SMγ-actin throughout the cytoplasm in the absence of SMα-actin. The compensatory increase in SMγ-actin could potentially contribute to increase stiffness of *Acta2*$^{-/-}$ cells,[33] but is not able to restore cellular contractile properties. These findings are in agreement with the observations that *Acta2*$^{-/-}$ mice have lower systolic blood pressure measured by noninvasive tail cuff and impaired aortic vascular contractility in response to potassium chloride, norepinephrine, and serotonin *in vitro*.[35] Kwartler et al.[65] subsequently reported that responses to phenylephrine and potassium chloride were significantly impaired in aortic rings from *Acta2*$^{-/-}$ mice. Bersi *et al*.[66] also reported larger outer diameters for carotid arteries from *Acta2*$^{-/-}$ mice compared with controls at perfusion pressures above 90 mmHg. Collectively, our results and others show that adaptive responses to stretch or pressure are impaired when SMα-actin filaments are disrupted.

SMCs are responsible for secreting the matrix *in vivo* and organizing it through force-dependent processes that involve both actin cytoskeleton and integrins at cell–matrix adhesions. Thus, external mechanical stresses are balanced by intracellular counter-forces provided by the actomyosin apparatus that forms stress fibers.[3,4] *In vitro* controlled 3D environments represent a useful tool to dissect the functional mechanosensing ability of *Acta2*$^{-/-}$ cells and their discrete contribution to tissue mechanical properties. By embedding live cells in collagen gels, we found that *Acta2*$^{-/-}$ cells exhibit impaired capacity to remodel local collagen fiber distribution. While WT cells appear to be able to exert tension on the collagen fibers and align them along a preferred axis, *Acta2*$^{-/-}$ cells were unable to remodel the collagen fibers. The reduced interaction with the matrix can be due to reduced contractility due to loss of SMα-actin and/or reduced cell adhesion to the extracellular matrix. Because SMC attachment to the matrix is essential in maintaining the functional and structural integrity of the vessel wall, dysfunctional cell adhesion to the matrix can lead to detachments of the SMC layer from the surrounding matrix compromising the structural integrity of the vessel wall.[28,60]

Changes in transmural pulse pressure are sensed by integrin receptors on the cell surface at the interface with the matrix. These receptors transmit mechanical stimulation intracellularly to the actomyosin contractile unit. Our results showed that loss of SMα-actin is associated with reduced integrin recruitment at cell matrix adhesions for both RGD-binding integrins $\alpha5\beta1$ and $\alpha v\beta3$, and collagen-binding integrin $\alpha2\beta1$ in *Acta2*$^{-/-}$ cells. Reduced recruitment of $\alpha2$ integrin at cell–matrix adhesions explains the inability of *Acta2*$^{-/-}$ cells to crosstalk and remodel the collagen matrix. Functional localization of $\alpha5$ integrin towards the center of the cell (i.e. at fibrillar adhesions) associates with fibronectin fibrillogenesis[67] and the ability of these integrins to sustain force.[68] The differential distribution of this integrin at the basal cell surface between *Acta2*$^{-/-}$ vs. WT cells and absence of SMα-actin that reinforces these adhesions, coupled with the role of this integrin in regulating vessel wall contractility,[16–17] support the reduced contractility of the aortic rings from *Acta2*$^{-/-}$mice.

Decreased SMC attachment to the matrix was also observed in the *Acta2*$^{-/-}$ aortas by electron microscopy.[69] While the SMCs in aortas from WT mice were aligned along the elastin fibers, the SMCs in aortas from *Acta2*$^{-/-}$ mice were improperly oriented with respect to the elastin fibers. Elastin fibers are covered with a sheath of elastic microfibrils composed of fibrilin glycoprotein. Fibrillin-1 presents a RGD-binding motif that mediates binding to integrins $\alpha v\beta3$, $\alpha v\beta6$, and $\alpha5\beta1$ with high-, moderate-, and low affinity, respectively.[23] Integrin $\alpha v\beta3$ has a role in initiating mechanotransduction at the leading edge of migrating cells. These integrins also mediate connection to the actin cytoskeleton, and adhesion reinforcement in response to external force.[68] Since $\alpha v\beta3$ integrin also binds with high affinity to elastin fibers, via fibrillin, the reduced recruitment of $\beta3$ integrin at peripheral cell–matrix adhesion in *Acta2*$^{-/-}$ cells may further explain the abnormal SMC attachment to the matrix visualized by electron microcopy *in vivo*, and may contribute to the reduced stress relaxation of the aortic rings from *Acta2*$^{-/-}$ mice. Taken together, these results support a reduced contractile phenotype and interaction with the matrix of *Acta2*$^{-/-}$ cells caused by the dysregulation of SMα-actin function, which in turn induces a cascade of molecular events affecting cellular mechanosensing.

ACKNOWLEDGEMENTS

The authors acknowledge the assistance of Dr. Malea M. Murphy for smooth muscle γ-actin imaging at the Integrated Microscopy and Imaging Laboratory, Texas A&M University Health Science Center, Bryan, TX. Authors thank Frida Leon Olmedo, undergraduate student in the Department of Biomedical Engineering, Texas A&M University and member of AT lab, for her contribution to the analysis of single cell fluorescence images.

Authors' contributions: AT, MPM, DMM, ATY and GMR conceived the study or analyzed the data and wrote/edited the manuscript. MPM, BCB, HCG, SP, JC, and JPT collected and/or analyzed the data and wrote/edited the manuscript.

DECLARATION OF CONFLICTING INTERESTS

The author(s) declared no potential conflicts of interest with respect to the research, authorship, and/or publication of this article.

FUNDING

This work was supported by the AHA award 18TPA34230049 to A.T., and NIH grants R01HL146583 and R01HL109942 to D.M.M.

ORCID IDS

MP Massett https://orcid.org/0000-0001-5356-4959
A Trache https://orcid.org/0000-0002-2070-4895

REFERENCES

1. Olson EN, Nordheim A. Linking actin dynamics and gene transcription to drive cellular motile functions. *Nat Rev Mol Cell Biol* 2010;**11**:353–65
2. Chen Y, Pasapera AM, Koretsky AP, Waterman CM. Orientation-specific responses to sustained uniaxial stretching in focal adhesion growth and turnover. *Proc Natl Acad Sci U S A* 2013;**110**:E2352–61
3. Ingber DE. Cellular mechanotransduction: putting all the pieces together again. *FASEB J* 2006;**20**:811–27
4. Wang N, Naruse K, Stamenovic D, Fredberg JJ, Mijailovich SM, Toric-Norrelykke IM, Polte T, Mannix R, Ingber DE. Mechanical behavior in living cells consistent with the tensegrity model. *Proc Natl Acad Sci U S A* 2001;**98**:7765–70
5. Rhodin JAG. Architecture of the vessel wall. *Comprehen Physiol* 2014;**2**(1):1–31
6. Turner CE, Kramarcy N, Sealock R, Burridge K. Localization of paxillin, a focal adhesion protein, to smooth muscle dense plaques, and the myotendinous and neuromuscular junctions of skeletal muscle. *Exp Cell Res* 1991;**192**:651–5
7. Alenghat FJ, Ingber DE. Mechanotransduction: all signals point to cytoskeleton, matrix, and integrins. *Sci STKE* 2002;**2002**:pe6
8. Geiger B, Bershadsky A. Assembly and mechanosensory function of focal contacts. *Curr Opin Cell Biol* 2001;**13**:584–92
9. Zamir E, Geiger B. Molecular complexity and dynamics of cell-matrix adhesions. *J Cell Sci* 2001;**114**:3583–90
10. del Rio A, Perez-Jimenez R, Liu R, Roca-Cusachs P, Fernandez JM, Sheetz MP. Stretching single talin rod molecules activates vinculin binding. *Science* 2009;**323**:638–41
11. Dumbauld DW, Lee TT, Singh A, Scrimgeour J, Gersbach CA, Zamir EA, Fu J, Chen CS, Curtis JE, Craig SW, Garcia AJ. How vinculin regulates force transmission. *Proc Natl Acad Sci U S A* 2013;**110**:9788–93
12. Zaidel-Bar R, Itzkovitz S, Ma'ayan A, Iyengar R, Geiger B. Functional atlas of the integrin adhesome. *Nat Cell Biol* 2007;**9**:858–67
13. Kuo JC, Han X, Hsiao CT, Yates JR, 3rd, Waterman CM. Analysis of the myosin-II-responsive focal adhesion proteome reveals a role for beta-Pix in negative regulation of focal adhesion maturation. *Nat Cell Biol* 2011;**13**:383–93
14. Martinez-Lemus LA, Sun Z, Trache A, Trzciakowski JP, Meininger GA. Integrins and regulation of the microcirculation: from arterioles to molecular studies using atomic force microscopy. *Microcirculation* 2005;**12**:99–112
15. Martinez-Lemus LA, Wu X, Wilson E, Hill MA, Davis GE, Davis MJ, Meininger GA. Integrins as unique receptors for vascular control. *J Vasc Res* 2003;**40**:211–33
16. Wu X, Mogford JE, Platts SH, Davis GE, Meininger GA, Davis MJ. Modulation of calcium current in arteriolar smooth muscle by alphav beta3 and alpha5 beta1 integrin ligands. *J Cell Biol* 1998;**143**:241–52
17. Wu X, Davis GE, Meininger GA, Wilson E, Davis MJ. Regulation of the L-type calcium channel by alpha5 beta1 integrin requires signaling between focal adhesion proteins. *J Biol Chem* 2001;**276**:30285–92
18. D'Angelo G, Mogford JE, Davis GE, Davis MJ, Meininger GA. Integrin-mediated reduction in vascular smooth muscle [Ca2+]i induced by RGD-containing peptide. *Am J Physiol* 1997;**272**:H2065–70
19. Schnapp LM, Goswami S, Rienzi N, Koteliansky VE, Gotwals P, Schachter EN. Integrins inhibit angiotensin II-induced contraction in rat aortic rings. *Regul Pept* 1998;**77**:177–83
20. Lim SM, Kreipe BA, Trzeciakowski J, Dangott L, Trache A. Extracellular matrix effect on RhoA signaling modulation in vascular smooth muscle cells. *Exp Cell Res* 2010;**316**:2833–48
21. Rensen SS, Doevendans PA, van Eys GJ. Regulation and characteristics of vascular smooth muscle cell phenotypic diversity. *Neth Heart J* 2007;**15**:100–8
22. Pfaff M, Reinhardt DP, Sakai LY, Timpl R. Cell adhesion and integrin binding to recombinant human fibrillin-1. *FEBS Lett* 1996;**384**:247–50
23. Jovanovic J, Iqbal S, Jensen S, Mardon H, Handford P. Fibrillin-integrin interactions in health and disease. *Biochem Soc Trans* 2008;**36**:257–62
24. Karimi A, Milewicz DM. Structure of the elastin-contractile units in the thoracic aorta and how genes that cause thoracic aortic aneurysms and dissections disrupt this structure. *Can J Cardiol* 2016;**32**:26–34
25. Kuang SQ, Kwartler CS, Byanova KL, Pham J, Gong L, Prakash SK, Huang J, Kamm KE, Stull JT, Sweeney HL, Milewicz DM. Rare, non-synonymous variant in the smooth muscle-specific isoform of myosin heavy chain, MYH11, R247C, alters force generation in the aorta and phenotype of smooth muscle cells. *Circ Res* 2012;**110**:1411–22
26. Wang L, Guo DC, Cao J, Gong L, Kamm KE, Regalado E, Li L, Shete S, He WQ, Zhu MS, Offermanns S, Gilchrist D, Elefteriades J, Stull JT, Milewicz DM. Mutations in myosin light chain kinase cause familial aortic dissections. *Am J Hum Genet* 2010;**87**:701–7
27. Guo DC, Regalado E, Casteel DE, Santos-Cortez RL, Gong L, Kim JJ, Dyack S, Horne SG, Chang G, Jondeau G, Boileau C, Coselli JS, Li Z, Leal SM, Shendure J, Rieder MJ, Bamshad MJ, Nickerson DA, Gen T, National Heart L, Blood Institute Grand Opportunity Exome Sequencing P, Kim C, Milewicz DM. Recurrent gain-of-function mutation in PRKG1 causes thoracic aortic aneurysms and acute aortic dissections. *Am J Hum Genet* 2013;**93**:398–404
28. Guo DC, Pannu H, Tran-Fadulu V, Papke CL, Yu RK, Avidan N, Bourgeois S, Estrera AL, Safi HJ, Sparks E, Amor D, Ades L, McConnell V, Willoughby CE, Abuelo D, Willing M, Lewis RA, Kim DH, Scherer S, Tung PP, Ahn C, Buja LM, Raman CS, Shete SS, Milewicz DM. Mutations in smooth muscle alpha-actin (ACTA2) lead to thoracic aortic aneurysms and dissections. *Nat Genet* 2007;**39**:1488–93
29. Lu H, Fagnant PM, Bookwalter CS, Joel P, Trybus KM. Vascular disease-causing mutation R258C in ACTA2 disrupts actin dynamics and interaction with myosin. *Proc Natl Acad Sci U S A* 2015;**112**:E4168–77
30. Lu H, Fagnant PM, Krementsova EB, Trybus KM. Severe molecular defects exhibited by the R179H mutation in human vascular smooth muscle alpha-Actin. *J Biol Chem* 2016;**291**:21729–39
31. Bellini C, Bersi MR, Caulk AW, Ferruzzi J, Milewicz DM, Ramirez F, Rifkin DB, Tellides G, Yanagisawa H, Humphrey JD. Comparison of 10 murine models reveals a distinct biomechanical phenotype in thoracic aortic aneurysms. *J R Soc Interface* 2017;**14**:20161036
32. Criado FJ. Aortic dissection: a 250-year perspective. *Tex Heart Inst J* 2011;**38**:694–700
33. Papke CL, Cao J, Kwartler CS, Villamizar C, Byanova KL, Lim SM, Sreenivasappa H, Fischer G, Pham J, Rees M, Wang M, Chaponnier C, Gabbiani G, Khakoo AY, Chandra J, Trache A, Zimmer W, Milewicz DM. Smooth muscle hyperplasia due to loss of smooth muscle alpha-actin is driven by activation of focal adhesion kinase, altered p53 localization and increased levels of platelet- derived growth factor receptor-beta. *Hum Mol Genet* 2013;**22**:3123–37
34. Humphrey JD, Milewicz DM, Tellides G, Schwartz MA. Cell biology. Dysfunctional mechanosensing in aneurysms. *Science* 2014;**344**:477–9
35. Schildmeyer LA, Braun R, Taffet G, Debiasi M, Burns AE, Bradley A, Schwartz RJ. Impaired vascular contractility and blood pressure homeostasis in the smooth muscle alpha-actin null 16 mouse. *FASEB J* 2000;**14**:2213–20
36. Humphrey JD. *Continuum mechanics. Cardiovascular solid mechanics*. Berlin, Germany: Springer, 2002, pp. 68–106
37. Bellini C, Wang S, Milewicz DM, Humphrey JD. Myh11(R247C/R247C) mutations increase thoracic aorta vulnerability to intramural damage despite a general biomechanical adaptivity. *J Biomech* 2015;**48**:113–21
38. Mulvany MJ, Halpern W. Contractile properties of small arterial resistance vessels in spontaneously hypertensive and normotensive rats. *Circ Res* 1977;**41**:19–26
39. Wheeler JB, Mukherjee R, Stroud RE, Jones JA, Ikonomidis JS. Relation of murine thoracic aortic structural and cellular changes with aging to passive and active mechanical properties. *J Am Heart Assoc* 2015;**4**: e001744
40. Wright GL, Battistella-Patterson AS. Involvement of the cytoskeleton in calcium-dependent stress relaxation of rat aortic smooth muscle. *J Muscle Res Cell Motil* 1998;**19**:405–14

41. Cao J, Gong L, Guo DC, Mietzsch U, Kuang SQ, Kwartler CS, Safi H, Estrera A, Gambello MJ, Milewicz DM. Thoracic aortic disease in tuberous sclerosis complex: molecular pathogenesis and potential therapies in Tsc2+/- mice. *Hum Mol Genet* 2010;**19**:1908–20
42. Seawright JW, Sreenivasappa H, Gibbs HC, Padgham S, Shin SY, Chaponnier C, Yeh AT, Trzeciakowski JP, Woodman CR, Trache A. Vascular smooth muscle contractile function declines with age in skeletal muscle feed arteries. *Front Physiol* 2018;**9**:856
43. Larson AM, Yeh AT. Ex vivo characterization of sub-10-fs pulses. *Opt Lett* 2006;**31**:1681–3
44. Schindelin J, Arganda-Carreras I, Frise E, Kaynig V, Longair M, Pietzsch T, Preibisch S, Rueden C, Saalfeld S, Schmid B, Tinevez JY, White DJ, Hartenstein V, Eliceiri K, Tomancak P, Cardona A. Fiji: an open-source platform for biological-image analysis. *Nat Methods* 2012;**9**:676–82
45. Schneider CA, Rasband WS, Eliceiri KW. NIH image to ImageJ: 25 years of image analysis. *Nat Methods* 2012;**9**:671–5
46. Peng H, Ruan Z, Long F, Simpson JH, Myers EW. V3D enables real-time 3D visualization and quantitative analysis of large-scale biological image data sets. *Nat Biotechnol* 2010;**28**:348–53
47. Chaudhuri S, Nguyen H, Rangayyan RM, Walsh S, Frank CB. A Fourier domain directional filtering method for analysis of collagen alignment in ligaments. *IEEE Trans Biomed Eng* 1987;**34**:509–18
48. Bai Y, Lee PF, Gibbs HC, Bayless KJ, Yeh AT. Dynamic multicomponent engineered tissue reorganization and matrix deposition measured with an integrated nonlinear optical microscopy-optical coherence microscopy system. *J Biomed Opt* 2014;**19**:36014
49. Mohammadi H, Arora PD, Simmons CA, Janmey PA, McCulloch CA. Inelastic behaviour of collagen networks in cell-matrix interactions and mechanosensation. *J R Soc Interface* 2015;**12**:20141074
50. Hu JJ, Humphrey JD, Yeh AT. Characterization of engineered tissue development under biaxial stretch using nonlinear optical microscopy. *Tissue Eng Part A* 2009;**15**:1553–64
51. Mochitate K, Pawelek P, Grinnell F. Stress relaxation of contracted collagen gels: disruption of actin filament bundles, release of cell surface fibronectin, and down-regulation of DNA and protein synthesis. *Exp Cell Res* 1991;**193**:198–207
52. Sun Z, Martinez-Lemus LA, Trache A, Trzeciakowski JP, Davis GE, Pohl U, Meininger GA. Mechanical properties of the interaction between fibronectin and alpha5beta1-integrin on vascular smooth muscle cells studied using atomic force microscopy. *Am J Physiol Heart Circ Physiol* 2005;**289**:H2526–35
53. Arnoldi R, Hiltbrunner A, Dugina V, Tille JC, Chaponnier C. Smooth muscle actin isoforms: a tug of war between contraction and compliance. *Eur J Cell Biol* 2013;**92**:187–200
54. Chaponnier C, Gabbiani G. Monoclonal antibodies against muscle actin isoforms: epitope dentification and analysis of isoform expression by immunoblot and immunostaining in normal and regenerating skeletal muscle. *F1000Res* 2016;**5**:416
55. Trache A, Meininger GA. Total internal reflection fluorescence (TIRF) microscopy. *Curr Protoc Microbiol* 2008;**2**(2A):1–22
56. Trache A, Lim SM. Integrated microscopy for real-time imaging of mechanotransduction studies in live cells. *J Biomed Opt* 2009;**14**:034024
57. Ballestrem C, Hinz B, Imhof BA, Wehrle-Haller B. Marching at the front and dragging behind: differential alphaVbeta3-integrin turnover regulates focal adhesion behavior. *J Cell Biol* 2001;**155**:1319–32
58. Sehgel NL, Sun Z, Hong Z, Hunter WC, Hill MA, Vatner DE, Vatner SF, Meininger GA. Augmented vascular smooth muscle cell stiffness and adhesion when hypertension is superimposed on aging. *Hypertension* 2015;**65**:370–7
59. Sehgel NL, Vatner SF, Meininger GA. Smooth muscle cell stiffness syndrome"-revisiting the structural basis of arterial stiffness. *Front Physiol* 2015;**6**:335
60. Humphrey JD, Schwartz MA, Tellides G, Milewicz DM. Role of mechanotransduction in vascular biology: focus on thoracic aortic aneurysms and dissections. *Circ Res* 2015;**116**:1448–61
61. Owens GK. Regulation of differentiation of vascular smooth muscle cells. *Physiol Rev* 1995;**75**:487–517
62. Saga H, Kimura K, Hayashi K, Gotow T, Uchiyama Y, Momiyama T, Tadokoro S, Kawashima N, Jimbou A, Sobue K. Phenotype-dependent expression of alpha-smooth muscle actin in visceral smooth muscle cells. *Exp Cell Res* 1999;**247**:279–92
63. Cluzel C, Saltel F, Lussi J, Paulhe F, Imhof BA, Wehrle-Haller B. The mechanisms and dynamics of (alpha)v(beta)3 integrin clustering in living cells. *J Cell Biol* 2005;**171**:383–92
64. Nagayama K, Yanagihara S, Matsumoto T. Actin filaments affect on not only elasticity but also late viscous response in stress relaxation of single isolated aortic smooth muscle cells. *J Biomech Sci Eng* 2007;**2**:93–104
65. Kwartler CS, Gong L, Chen J, Wang S, Kulmacz R, Duan XY, Janda A, Huang J, Kamm KE, Stull JT, Guo D, Milewicz DM. Variants of unknown significance in genes associated with heritable thoracic aortic disease can be low penetrant "risk variants". *Am J Hum Genet* 2018;**103**:138–43
66. Bersi MR, Ferruzzi J, Eberth JF, Gleason RL, Jr., Humphrey JD. Consistent biomechanical phenotyping of common carotid arteries from seven genetic, pharmacological, and surgical mouse models. *Ann Biomed Eng* 2014;**42**:1207–23
67. Huveneers S, Truong H, Fassler R, Sonnenberg A, Danen EH. Binding of soluble fibronectin to integrin alpha5 beta1-link to focal adhesion redistribution and contractile shape. *J Cell Sci* 2008;**121**:2452–62
68. Roca-Cusachs P, Gauthier NC, Del Rio A, Sheetz MP. Clustering of alpha(5)beta(1) integrins determines adhesion strength whereas alpha (v)beta(3) and talin enable mechanotransduction. *Proc Natl Acad Sci U S A* 2009;**106**:16245–50
69. Chen J, Peters A, Papke CL, Villamizar C, Ringuette LJ, Cao J, Wang S, Ma S, Gong L, Byanova KL, Xiong J, Zhu MX, Madonna R, Kee P, Geng YJ, Brasier AR, Davis EC, Prakash S, Kwartler CS, Milewicz DM. Loss of smooth muscle alpha-Actin leads to NF-kappaB-Dependent increased sensitivity to angiotensin II in smooth muscle cells and aortic enlargement. *Circ Res* 2017;**120**:1903–15

(Received October 28, 2019, Accepted January 8, 2020)